Atmos. Chem. Phys., 24, 6525–6538, 2024
https://doi.org/10.5194/acp-24-6525-2024

Atmospheric Chemistry and Physics
Open Access
EGU

Non-negligible secondary contribution to brown carbon in autumn and winter: inspiration from particulate nitrated and oxygenated aromatic compounds in urban Beijing

Yanqin Ren[1], Zhenhai Wu[1], Yuanyuan Ji[1], Fang Bi[1], Junling Li[1], Haijie Zhang[1], Hao Zhang[1], Hong Li[1], and Gehui Wang[2]

[1]State Key Laboratory of Environmental Criteria and Risk Assessment, Chinese Research Academy of Environmental Sciences, Beijing 100012, China
[2]Key Lab of Geographic Information Science of Ministry of Education of China, School of Geographic Sciences, East China Normal University, Shanghai 200142, China

Correspondence: Hong Li (lihong@craes.org.cn) and Gehui Wang (ghwang@geo.ecnu.edu.cn)

Received: 3 November 2023 – Discussion started: 3 January 2024
Revised: 23 March 2024 – Accepted: 23 April 2024 – Published: 4 June 2024

Abstract. Nitrated aromatic compounds (NACs) and oxygenated derivatives of polycyclic aromatic hydrocarbons (OPAHs) play vital roles within brown carbon (BrC), influencing both climate dynamics and human health to a certain degree. The concentrations of these drug classes were analyzed in $PM_{2.5}$ from an urban area in Beijing during the autumn and winter of 2017 and 2018. There were four heavy haze episodes during the campaign, two of which happened prior to heating and the other two during heating. During the entire course of sampling, the mean total concentrations of the nine NACs and the eight OPAHs were 1.2–263 and 2.1–234 ng m^{-3}, respectively. The concentrations of both NACs and OPAHs were approximately 2–3 times higher in the heating period than before heating. For NACs, the relative molecular composition did not change significantly before and during heating, with 4-nitrocatechol and 4-nitrophenol demonstrating the highest abundance. For OPAHs, 1-naphthaldehyde was the most abundant species before and during heating, while the relative proportion of anthraquinone increased by more than twice, from 13 % before heating to 31 % during the heating. In Beijing's urban area during autumn and winter, significant sources of NACs and OPAHs have been traced back to automobile emissions and biomass burning activities. Interestingly, it was observed that the contribution from coal combustion increased notably during heating. It is worth noting that the secondary generation of BrC was important throughout the whole sampling period, which was manifested by the photochemical reaction before heating and the aqueous reaction during heating. It was further found that the haze in autumn and winter was nitrate-driven before heating and secondary organic carbon (SOC)-driven during heating, and the secondary formation of BrC increased significantly in pollution events, particularly during heating.

1 Introduction

As an important light-absorbing material, brown carbon (BrC) has garnered increasing attention in recent years (Jiang et al., 2023; Song et al., 2022; W. Zhang et al., 2021; Liu et al., 2023; Ren et al., 2023, 2022; Chen et al., 2022). BrC not only directly absorbed solar energy but also indirectly contributed to climate change by promoting the evaporation of water and the dispersal of clouds (Laskin et al., 2015; Huang et al., 2018). BrC also has potential adverse effects on human health on account of its strong mutagenic, cytotoxic, and carcinogenic properties (Teich et al., 2016).

Primary as well as secondary sources contribute to the atmospheric accumulation of BrC (Zhu et al., 2021). Direct

emissions of primary BrC come from biomass burning and the combustion of fossil fuels (Ni et al., 2021; H. Wang et al., 2020; Lu et al., 2019a, b). Secondary BrC in the atmosphere is produced from oxidation and aging processes (Y. Wang et al., 2019, 2020b; Cheng et al., 2021; Jiang et al., 2023; Cai et al., 2022). Toluene, phenol, benzene, and other aromatic hydrocarbons can be oxidized to produce nitrophenol or nitrocatechol by NO_3 or OH radical vapor phase in the presence of NO_x (Olariu et al., 2002; Sato et al., 2007; Iinuma et al., 2010; Ji et al., 2017). Volatile organic compounds (VOCs) can be oxidized to produce nitro-aromatic hydrocarbons when emitted during biomass combustion and pyrolysis (such as cresol, catechol, and methyl catechol) (Iinuma et al., 2010; Claeys et al., 2012; Finewax et al., 2018). Research on the source analysis of brown carbon (BrC) frequently focuses on examining two key constituents: the carbon component within humic-like substances (HULIS-C) and water-soluble organic carbon (WSOC). These components are often studied to understand the origins and properties of BrC in various environmental contexts. Secondary generation and burning of biomass are the two main sources of HULIS in Guangzhou and Shanghai (Fan et al., 2016; Zhao et al., 2016). In comparison with the water-insoluble BrC in the winter, the contribution of non-fossil sources (for instance burning biomass) to water-soluble BrC was sometimes as high as 70 % or more (Liu et al., 2018; Song et al., 2018). Coal combustion is presumably a significant source of HULIS in the winter, in addition to burning biomass and secondary generation (Tan et al., 2016). According to multiple studies conducted in Beijing, the primary contributor to WSOC is secondary generation, accounting for 54 % of its composition. Following this, biomass burning contributes approximately 40 %, while other primary emission sources contribute a smaller proportion, making up only 6 % (Du et al., 2014). In Beijing, the percentages of biomass burning, coal combustion, and secondary generation that contribute to atmospheric HULIS are 47 %, 15 %, and 39 %, respectively. The primary origins of HULIS show minimal association with motor vehicles and industrial emissions (Li et al., 2019). According to Ma et al. (2018), secondary generation is responsible for over 50 % of HULIS in the non-heating season. Biomass burning represents 21 % of the HULIS content during this period. However, in the heating season, approximately 40 % of HULIS originates from biomass burning, while the remaining 60 % is contributed by diverse combustion sources like coal burning, waste incineration, and vehicular emissions. Within this season, secondary generation accounts for about 19 % of the HULIS content (Ma et al., 2018).

The research suggests that various sources contribute to BrC, but their relative impact varies depending on time and location. As a result, the chemical makeup, light absorption characteristics, and concentrations of BrC show considerable variability. This variability poses challenges in accurately assessing and forecasting the influence of these sources on radiation and climate changes (Y. Wang et al., 2020a; Yan et al., 2018; Laskin et al., 2015). However, until recently, there was only a limited volume of research pertaining to the sources and pathways of BrC leading to their generation in the densely populated city environment. Nitrated aromatic compounds (NACs) and oxygenated derivatives of polycyclic aromatic hydrocarbons (OPAHs) are the primary focus of this study because several studies have noted that nitrogen-containing aromatics, polycyclic aromatic hydrocarbons (PAHs), and their derivatives are significant BrC chromophores (Huang et al., 2018; Wu et al., 2020; Liu et al., 2023; Y. Wang et al., 2020a; Xie et al., 2017). The average contribution of OPAHs (five species) to the solar-spectrum-weighted absorption coefficient of water-insoluble BrC in summer is 0.51 ± 0.28 % during daytime and 0.34 ± 0.19 % during nighttime. The contribution of NACs to light absorption of water-soluble BrC is on average 2.5 times higher during nighttime (3.47 ± 2.03 %) than during the day (1.41 ± 0.29 %) in winter, and the fractions are much higher in winter than in summer (0.12 ± 0.03 %) (J. Li et al., 2020). It is well-established that residential heating plays a significant role in the substantial increase of anthropogenic pollutant emissions during the winter season. There is a substantial rise in the emission of aromatics-derived secondary organic aerosol from autumn to winter (Ding et al., 2017), and particle BrC is often detected, especially in haze periods (Liu et al., 2023). This study was conducted in the autumn and winter of 2017 and 2018 in Beijing. Nine NACs and eight OPAHs were measured in $PM_{2.5}$ samples, with a focus on examining their sources, compositions, and concentration variations under various air conditions. Specifically, emphasis was placed on investigating the contribution of secondary generation to these two typical BrC species, particularly their involvement in particle pollution processes during autumn and winter.

2 Materials and methods

2.1 Field observations

$PM_{2.5}$ was sampled at a height of 10 m on the rooftop of a building at the Chinese Research Academy of Environmental Sciences (CRAES), Beijing, China (40°02′ N, 116°24′ E). Using a high-volume sampler ($1.13\ m^3\ min^{-1}$, Thermo Fisher Co., USA), $PM_{2.5}$ specimens were collected in the autumn and winter of 2017 and 2018. The sampling process was executed from 08:00 to 19:30 local time (LT) during the day and from 20:00 to 07:30 LT in the subsequent morning. The specimens and blanks were gathered using a pre-combusted quartz fiber filter (at 450 °C for 6 h). A total of four field blanks and 122 $PM_{2.5}$ samples were acquired. Individual filters were sealed in a bag made from an aluminum foil bag before sampling and analysis and placed in a freezer set at a temperature of −20 °C.

Using automatic equipment (CRAES Supersite for Comprehensive Urban Air Observation and Research), meteoro-

logical parameters such as air temperature (T; °C) and relative humidity (RH; %), along with gaseous pollutants (SO_2, NO_2, O_3, and CO), were observed and measured at the same time.

2.2 Chemical analysis

The present study employed a pre-treatment comprising ultrasonic extraction and derivatization in an attempt to analyze the organic species in the specimens. The details of specimen extraction and derivatization have already been published (Wang et al., 2009; Ren et al., 2021, 2023). In brief, filter aliquots were sectioned and extracted with a methanol and dichloromethane (1 : 2 v/v) mixture. Following the concentration of the extracts to dryness, derivatization was carried out using a mixture of N, O-bis-(trimethylsilyl) trifluoroacetamide [BSTFA + TMCS, (99 : 1), v/v] and pyridine (5 : 1, v/v). Lastly, the derivatized samples were examined using gas chromatography coupled with a mass spectroscopy detector (GC/MS: HP 7890A, HP 5975C, Agilent Co., USA). The extraction and derivatization methods described above allowed for the simultaneous measurement of the samples' polar and non-polar constituents.

Given that OPAHs and NACs were the main points of focus, this study investigated a total of eight OPAHs and nine NACs. The nine NACs included 2,4-dinitrophenol (2, 4-DNP), 4-nitrophenol (4NP), 3-methyl-4-nitrophenol (3M4NP), 4-nitrocatechol (4NC), 4-methyl-5-nitrocatechol (4M5NC), 4-nitroguaiacol (4NGA), 5-nitroguaiacol (5NGA), 3-nitro-salicylic acid (3NSA), and 5-nitro-salicylic acid (5NSA), while the eight OPAHs encompassed 9-fluorenone (9-FO), benzanthrone (BZA), 1-naphthaldehyde (1-NapA), anthraquinone (ATQ), 1,4-chrysenequione (1,4-CQ), benzo(a)anthracene-7,12-dione (7,12-BaAQ), 5,12-naphthacenequione (5,12-NAQ), and 6H-benzo(cd)pyrene-6-one (BPYRone).

The elemental carbon (EC) and organic carbon (OC) content of individual $PM_{2.5}$ filter samples were analyzed using an Atmoslytic Inc. DRI model 2001 carbon analyzer. This analysis followed the Interagency Monitoring of Protected Visual Environments (IMPROVE) thermal–optical reflectance (TOR) protocol, involving the examination of a 0.526 cm^2 punch from each specimen. The specifics of the above-described techniques have been documented in literature (Li et al., 2016; Ren et al., 2021).

2.3 Evaluation of secondary BrC

In this study, the contributions of secondary oxidation to the detected NACs and OPAHs were evaluated using a CO-tracer method, which is comparable to the EC tracer used for secondary OC quantification. Various methodologies have been similarly adopted successfully in other studies (Liu et al., 2023; Cai et al., 2022). Equations (1) and (2) were respectively used to evaluate the secondary formation of NACs and OPAHs.

$$[\mathrm{NACs}]_s = [\mathrm{NACs}]_t - ([\mathrm{NACs}]_t/[\mathrm{CO}])_{pri} \times [\mathrm{CO}] \quad (1)$$

$$[\mathrm{OPAHs}]_s = [\mathrm{OPAHs}]_t - ([\mathrm{OPAHs}]_t/[\mathrm{CO}])_{pri} \times [\mathrm{CO}] \quad (2)$$

$[\mathrm{NACs}]_s$ and $[\mathrm{NACs}]_t$ in Eq. (1) refer to the NAC concentration produced by secondary oxidation and the total amount of NACs, respectively. $([\mathrm{NACs}] / [\mathrm{CO}])_{pri}$ represents the primary emission ratio of NACs in relation to combustion. This calculation assumes that the primary source was predominant during the period, with minimal secondary production. The $([\mathrm{NACs}] / [\mathrm{CO}])_{pri}$ was calculated in this work by fitting the 15 % lowest $[\mathrm{NACs}]_t / [\mathrm{CO}]$ ratios observed during the entire sampling duration. In Eq. (2) the concentration of OPAHs produced by secondary oxidation and the total observed OPAHs are denoted by $[\mathrm{OPAHs}]_s$ and $[\mathrm{OPAHs}]_t$, respectively. The concentration of CO is denoted by [CO], while the primary emission ratio of OPAHs in relation to combustion is represented by $([\mathrm{OPAHs}] / [\mathrm{CO}])_{pri}$, which was calculated by fitting the lowest 15 % $[\mathrm{OPAHs}]_t / [\mathrm{CO}]$ ratios observed in the entire sample interval.

3 Results and discussion

3.1 Variations in major components of $PM_{2.5}$ with respect to meteorological conditions and gaseous pollution

Based on the Beijing heating time, the entire period of the study was divided into two phases: before heating (18 October to 14 November 2017) and during heating (15 to 23 November 2017; 23 December 2017 to 17 January 2018). Table 1 and Fig. 1 present the temporal fluctuations in meteorological factors, gaseous pollutant concentrations, and the main $PM_{2.5}$ components in the two phases. The temperature (T) and relative humidity (RH) were higher before heating (11 ± 3.8 °C and 49 ± 26 %) than during heating (1.9 ± 4.4 °C and 23 ± 15 %), with average values amounting to 5.9 ± 5.9 °C and 35 ± 25 %, respectively. SO_2 concentrations during heating (4.3 ± 1.5 ppb) were more than twice that before heating (2.1 ± 0.8 ppb), presumably because of the increase in household coal burning for heating. The levels of NO_2 and NO remained consistent before and during heating, suggesting that these pollutants were minimally impacted by heating and were primarily influenced by mobile sources in Beijing. This pattern seems to remain stable in the short term.

Figure 2 shows the variation in the chemical makeup of $PM_{2.5}$ in the whole sampling period, before and during hearting, respectively. Secondary inorganic aerosols (SIAs; i.e. SO_4^{2-}, NH_4^+, and NO_3^-) were identified as the leading constituents of $PM_{2.5}$, followed by organic material (OM; 1.6 times OC), with an average of 31.5 % and 20.4 % in the whole sampling, respectively (Fig. 2a). Even though the $PM_{2.5}$ concentrations remained relatively stable during this

Table 1. Gaseous pollution concentrations and meteorological parameters and chemical constituents of $PM_{2.5}$ during the sampling periods in Beijing.

	The whole sampling $N = 122$	Before heating period 18 October–14 November 2017 $N = 56$	During heating period 15–23 November 2017 23 December 2017–17 January 2018 $N = 66$
Meteorological parameters			
Temperature, °C	5.9 ± 5.9 ((−7.5)–16)	11 ± 3.8 (1.2–16)	1.9 ± 4.4 ((−7.5)–11)
Relative humidity, %	35 ± 25 (7.1–99)	49 ± 26 (11–99)	23 ± 15 (7.1–67)
Gaseous pollutants, ppb			
SO_2	3.2 ± 1.6 (1.1–7.9)	2.1 ± 0.8 (1.1–4.8)	4.3 ± 1.5 (2.2–7.9)
NO_2	26 ± 13 (4.6–56)	25 ± 11 (4.6–43)	26 ± 14 (5.5–56)
NO	26 ± 28 (2.4–136)	28 ± 30 (2.4–136)	25 ± 26 (2.7–116)
CO	0.64 ± 0.55 (0.03–2.7)	0.81 ± 0.42 (0.12–1.6)	0.50 ± 0.61 (0.03–2.7)
Major components of $PM_{2.5}$, $\mu g\,m^{-3}$			
$PM_{2.5}$	65 ± 40 (6.1–195)	64 ± 39 (6.1–175)	66 ± 41 (8.6–195)
OC	8.3 ± 5.0 (0.99–26)	7.4 ± 3.9 (1.0–18)	9.1 ± 5.8 (1.8–26)
EC	4.7 ± 4.7 (0.11–25)	4.9 ± 3.8 (0.11–17)	4.5 ± 5.3 (0.18–25)
OC / EC	3.7 ± 3.6 (0.96–21)	2.7 ± 3.3 (0.96–21)	4.4 ± 3.7 (1.0–17)
SO_4^{2-}	4.8 ± 4.2 (0.85–25)	5.5 ± 3.5 (0.86–13)	4.3 ± 4.7 (0.85–25)
NO_3^-	11 ± 14 (0.09–58)	16 ± 16 (0.09–58)	6.8 ± 8.8 (0.29–37)
NH_4^+	4.7 ± 4.9 (0.02–20)	5.4 ± 5.4 (0.02–20)	4.2 ± 4.5 (0.19–20)
K^+	0.43 ± 0.39 (0.02–2.2)	0.38 ± 0.27 (0.03–1.1)	0.48 ± 0.46 (0.02–2.2)
Cl^-	1.5 ± 1.6 (0.06–9.2)	1.0 ± 0.98 (0.06–4.5)	1.9 ± 2.0 (0.13–9.2)

period (as indicated in Table 1 and Fig. 2), there were significant changes observed in the concentrations of SIA and OM, as well as their relative contributions to $PM_{2.5}$. SIA accounted for 41.9 % of $PM_{2.5}$ before heating, which notably decreased to 23.1 % during heating. This decline was primarily evident in the reduction of NO_3^-. SO_4^{2-}, NO_3^-, and NH_4^+ were measured at 5.5, 16, and 5.4 $\mu g\,m^{-3}$, respectively, which constituted 8.7 %, 24.7 %, and 8.5 % of $PM_{2.5}$ before heating (Fig. 2b). And their concentrations decreased to 4.3, 6.8, and 4.2 $\mu g\,m^{-3}$ (Table 1). The relative contributions of NO_3^- to $PM_{2.5}$ dropped dramatically to 10.3 % during heating, amounting to a drop of nearly 60 %. Both SO_4^{2-} and NH_4^+ experienced a roughly 25 % decrease in their relative contributions to $PM_{2.5}$, as illustrated in Fig. 2c. The relative abundance of OM to $PM_{2.5}$ increased from 18.6 % before heating to 21.9 % during heating, with the average mass concentration of OC showing an increase from 7.4 to 9.1 $\mu g\,m^{-3}$ in the corresponding duration. The OC / EC ratio also increased by 63 % from 2.7 ± 3.3 before heating to 4.4 ± 3.7 during heating. These significant changes in SIA and OM, including concentrations and the relative contributions to $PM_{2.5}$, showed that primary organic aerosols and/or VOCs emissions were the leading contributors during the heating seasons due to household heating (Tan et al., 2018). It is important to note that the decreased proportion of SIA in $PM_{2.5}$ may also be affected by meteorological conditions during heating, which often influence their production (Wang et al., 2016; An et al., 2019). For example, increased sulfate is often accompanied by a high RH in the urban atmosphere, and the reaction rate of nitrate formation is accelerated by increasing RH (Zhang et al., 2015; Sun et al., 2013). However, the RH was lower during heating than before heating. Aside from coal combustion, the rise in mass concentrations of K^+ and Cl^- indicated additional burning activities occurring during heating, such as biomass burning (Bai et al., 2023; Li et al., 2022).

3.2 Concentration and composition variations of BrC compounds

This work quantified nine NACs and eight OPAHs. The corresponding concentrations and compositions have been presented in Fig. 3 and Table S1 (Supplement).

As seen in Table S1, during the entire sampling, the total concentrations of NACs ($\sum$9NACs) and their corresponding contribution to OM ($\sum$9NACs / OM) respectively averaged 38 (1.2–263) ng m^{-3} and 0.25 % (0.03 %–0.86 %). $\sum$9NACs and $\sum$9NACs / OM respectively averaged 53 (4.5–263) ng m^{-3} and 0.33 % (0.09 %–0.86 %) during heating; both values are 2 times higher in magnitude in comparison to those measured before heating (average of 20 (1.2–108) ng m^{-3} and 0.15 % (0.03 %–0.4 %), respectively).

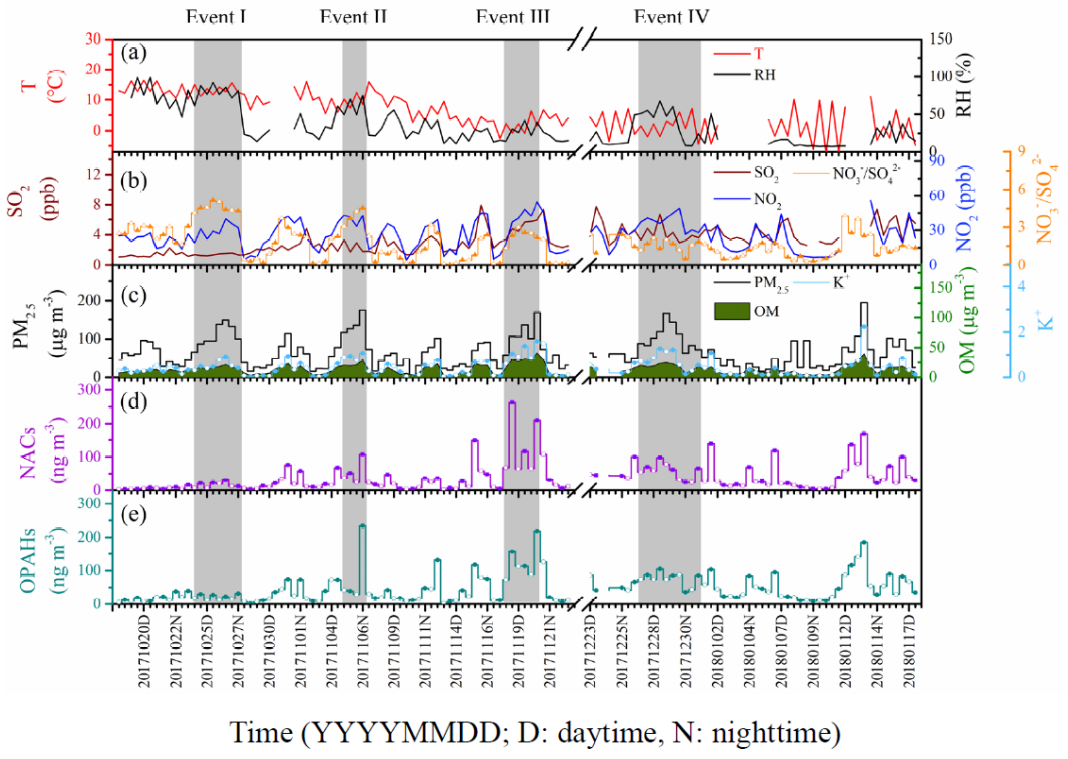

Figure 1. Time series of **(a)** RH and T; **(b)** SO_2 and NO_2; **(c)** $PM_{2.5}$, OM, and K^+; **(d)** NACs; and **(e)** OPAHs in the autumn and winter of urban Beijing. (Daytime is denoted by empty marks, and nighttime is represented by solid marks in the panels **(b)**–**(e)**. The pollution episodes, with elevated concentrations of daily $PM_{2.5}$ more than 75 $\mu g\,m^{-3}$ in two successive days, have been marked in light gray.)

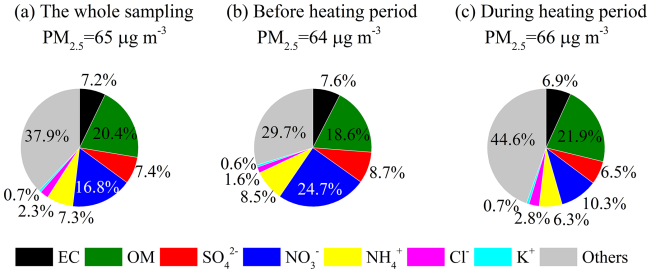

Figure 2. Chemical constitution of $PM_{2.5}$ in the entire sampling period **(a)** and before **(b)** and during **(c)** heating periods.

∑9NACs exhibited a nighttime increase, reaching approximately twice the levels observed during daytime throughout the entire campaign (Fig. 3a). The observed difference between day and night is consistent with our previous research (Ren et al., 2022). However, the relative molecular composition of the total nine NACs in $PM_{2.5}$ did not manifest any significant change (Fig. 4a, c). 4-Nitrophenol (4NP) was found to have the highest concentration among all species, accounting for 44 % and 42 % of the total NACs before and during heating, followed by 4-nitrocatechol (4NC), which accounted for 21 % before heating and 23 % during heating. These findings align with the dominant species observed in previous studies (Ren et al., 2022, 2023; X. Li et al., 2020). However, the values were much higher in comparison to those found in our earlier work (Ren et al., 2022) at the same sample site during the spring (8.6 (0.48–27) $ng\,m^{-3}$) and summer (8.5 (1.0–16) $ng\,m^{-3}$). It is plausible that seasonal variations in NACs are linked to emission sources, formation pathways, and weather conditions. In this study, the overall abundance of the ∑9NACs appeared to align closely with measurements from earlier studies conducted during winter in Beijing (74 ± 51 $ng\,m^{-3}$ in winter, 20 ± 12 $ng\,m^{-3}$ in autumn) (X. Li et al., 2020) and Jinan (48 ± 26 $ng\,m^{-3}$ in winter, 9.8 ± 4.2 $ng\,m^{-3}$ in autumn; Wang et al., 2018) but are significantly higher than those measured for Xi'an (17 ± 12 $ng\,m^{-3}$) and Hong Kong SAR (12 ± 14 $ng\,m^{-3}$) in winter (Wu et al., 2020; Chow et al., 2016). In contrast to studies conducted abroad, the levels of ∑9NACs in this particular study tended to be higher in Germany, at 16 $ng\,m^{-3}$, while in the UK, levels were around 19 $ng\,m^{-3}$. Belgium recorded levels of 32 $ng\,m^{-3}$ in winter and 13 $ng\,m^{-3}$ in autumn (Teich et al., 2017; Mohr et al., 2013; Kahnt et al., 2013). This indicates that it is urgent to further reduce the concentration of contaminant precursors in China.

Throughout the sampling, the total concentrations of OPAHs (∑8OPAHs) averaged 47 (1.2–234) $ng\,m^{-3}$, whereas the mean value for their total contribution to

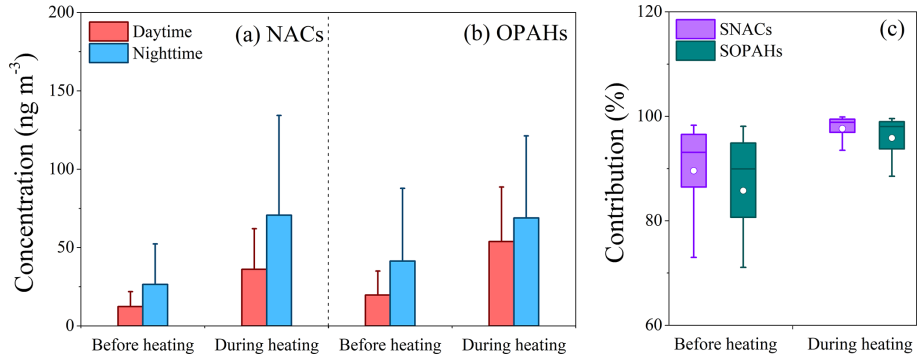

Figure 3. NAC and OPAH concentrations **(a, b)** and contributions of secondary formation (SNACs, SOPAHs) to the total **(c)**, before and during heating periods. The mean values are represented by the markers, and the 25th and 75th percentiles are represented by whiskers.

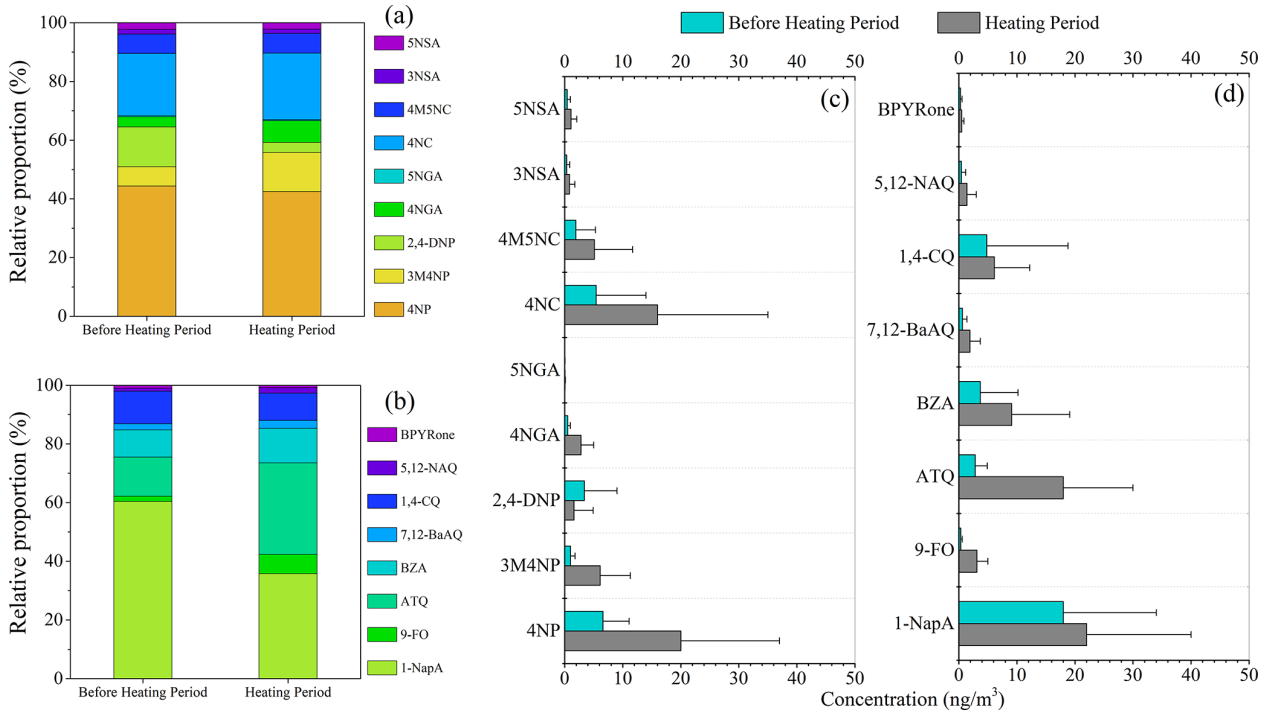

Figure 4. Comparison of measurements before and during the heating period at the urban site of Beijing, including **(a)** relative proportion of NAC species, **(b)** relative proportion of OPAH species, **(c)** NAC concentrations, and **(d)** OPAH concentrations. (4NP: 4-nitrophenol. 3M4NP: 3-methyl-4-nitrophenol. 2, 4-DNP: 2,4-dinitrophenol. 4NGA: 4-nitroguaiacol. 5NGA: 5-nitroguaiacol. 4NC: 4-nitrocatechol. 4M5NC: 4-methyl-5-nitrocatechol. 3NSA: 3-nitro-salicylic acid. 5NSA: 5-nitro-salicylic acid. 1-NapA: 1-naphthaldehyde. 9-FO: 9-fluorenone. ATQ: anthraquinone. BZA: benzanthrone. 7,12-BaAQ: benzo(a)anthracene-7,12-dione. 1,4-CQ: 1,4-chrysenequione. 5,12-NAQ: 5,12-naphthacenequione. BPYRone: 6H-benzo(cd)pyrene-6-one.)

OM ($\sum$8OPAHs / OM) was 0.33 % (0.06 %–0.81 %) (Table S1). These values were both slightly higher than those of NACs in this work. $\sum$8OPAHs and $\sum$8OPAHs / OM respectively averaged 61 (6.9–218) ng m^{-3} and 0.40 % (0.18 %–0.58 %) during heating. These values are almost twice as much as those measured before heating (averaging 31 (2.1–234) ng m^{-3} and 0.24 % (0.06 %–0.81 %), respectively). Like the $\sum$9NACs, the combined levels of $\sum$8OPAHs were higher during nighttime compared to daytime, averaging about twice as high before heating and 1.3 times during heating, as indicated in Fig. 3b. Among the eight OPAHs studied, 1-NapA constituted the highest proportion before (60 %) and during (36 %) heating. However, the relative proportion of ATQ more than doubled, increasing from 13 % before heating to 31 % during heating, as depicted in Fig. 4b and d. The average concentrations of $\sum$8OPAHs were higher than those recorded for other Chinese urban sites, including Guangzhou (23 ng m^{-3}) and Xi'an (54 ng m^{-3}) (Ren et al., 2017), as well

as higher than those documented for southern (41.8 ng m^{-3}, traffic site) (Alves et al., 2017) and central (~ 10 ng m^{-3}) European cities (Lammel et al., 2020). The average concentrations of ∑8OPAHs were also higher than those recorded for Mainz, Germany (0.047–1.6 ng m^{-3}), and Thessaloniki, Greece (0.86–4.3 ng m^{-3}) (Kitanovski et al., 2020).

3.3 Sources and formation of BrC compounds

The relation between individual and total species and the associated pollutants – levoglucosan, K^+, SO_2, NO_2, O_3, RH, and SIA – was examined according to the data findings for the Pearson correlations shown in Table 2 (for NACs) and Table 3 (for OPAHs) to provide additional clarity regarding the source and formation of NACs and OPAHs. There were strong correlations between levoglucosan (an organic tracer associated with biomass burning), K^+ (an inorganic tracer linked to biomass burning), and NO_2 with total NACs and all identified NAC species, which indicated that both automobile emissions and biomass burning played significant roles in the accumulation of NACs in urban Beijing throughout the entire campaign. The correlation between NACs and SO_2 was significantly higher during heating ($r = 0.275$, $p < 0.05$) compared to pre-heating ($r = 0.210$, $p > 0.05$), suggesting that coal combustion plays a more significant role in NAC formation after heating commences.

In addition to these primary pollutants, NACs were also significantly correlated with some secondary pollutants. Before heating, there existed a strong positive association ($r = 0.692$, $p < 0.01$) between NACs and O_3. However, this association changed considerably after heating, becoming notably negative ($r = -0.303$, $p < 0.05$). The negative correlation between them may be related to the meteorological conditions during the sampling period, e.g. lower temperature and weak solar irradiation, which suppress the photodegradation process of NACs (J. Li et al., 2020). NACs and RH concurrently displayed a strong positive correlation ($r = 0.548$, $p < 0.01$) during heating. Along with SO_4^{2-}, NO_3^-, and NH_4^+, total NACs also exhibited high positive correlation, particularly while heating ($r = 0.373$, $p < 0.01$; $r = 0.504$, $p < 0.01$; $r = 0.513$, $p < 0.01$, respectively). The overall concentrations of OPAHs and NACs throughout the campaign exhibited substantial correlations ($r = 0.830$, $p < 0.01$ before heating; $r = 0.895$, $p < 0.01$ during heating) (Table 3, Fig. S1). This suggests that their sources and/or influencing variables were comparable. Specifically, throughout the entire campaign, both total OPAHs and all identified OPAH species exhibited a strong correlation with levoglucosan, K^+, and NO_2. This implies that automobile emissions and biomass burning played significant roles as sources of OPAHs. OPAHs and SO_2 ($r = 0.365$, $p < 0.01$) were determined to be more strongly correlated during heating than before heating, suggesting the contribution of coal combustion to OPAHs becomes significant during heating. Moreover, the correlation between OPAHs and O_3 was significantly positive before heating ($r = 0.563$, $p < 0.01$), whereas it was significantly negative during heating ($r = -0.385$, $p < 0.01$). Furthermore, it was discovered that throughout the heating phase, OPAHs and RH had a substantial positive correlation ($r = 0.578$, $p < 0.01$). Total OPAHs also showed good correlations with SO_4^{2-}, NO_3^-, and NH_4^+, especially during the heating period ($r = 0.477$, $p < 0.01$; $r = 0.658$, $p < 0.01$; and $r = 0.658$, $p < 0.01$; respectively).

The observed phenomena, involving photooxidation before heating and aqueous reactions during heating, strongly suggest a significant role in the secondary creation of BrC throughout the entire sampling period. Earlier studies have highlighted that in certain regions, the primary mechanism driving the formation of nitro-aromatic hydrocarbons involves the gaseous-phase oxidation of VOC precursors from anthropogenic sources, such as toluene and benzene (Olariu et al., 2002; Sato et al., 2007; Yuan et al., 2016; Ji et al., 2017; Liu et al., 2023). According to a recent study, for instance, NACs are mostly generated at a rural location on China's Chongming Island through gaseous-phase photooxidation (Liu et al., 2023). Aqueous reaction is also a key pathway for the formation of BrC (Zhang et al., 2020; Cheng et al., 2021; Jiang et al., 2023). Previous studies suggested that aqueous-phase reaction is an important pathway for secondary BrC formation during the winter season (Zhang et al., 2020; J. Li et al., 2020). The field observations of Wang et al. (2019) in urban Beijing revealed that the aqueous reaction is a significant mechanism for the secondary synthesis of nitro-aromatic hydrocarbons during summer temperatures with high relative humidity. Furthermore, spherical primary OM particles (i.e., tar balls), which are mainly from residential coal burning, especially during the heating period in the North China Plain, usually contain BrC species, and their aqueous formation could occur during the long-range transport (J. Zhang et al., 2021, 2023).

From the above analysis, it is evident that there is a good correlation between these two aromatic compounds and levoglucosan, as long-lived and inert chemicals in the atmosphere (Cai et al., 2022). Therefore, it was not possible to determine with certainty whether NACs and OPAHs originated predominantly from direct emission from the biomass combustion or by secondary oxidation of the precursors produced as a result of the process. The outcomes of Eqs. (1) and (2) indicated that in Beijing's urban areas during autumn and winter, NACs and OPAHs were predominantly of secondary origin. Throughout the entire sampling period, secondary formation accounted for 17 % to 99 % (average of 80 %) of NACs and 8.9 % to 99 % (average of 73 %) of OPAHs, as depicted in Fig. 3c. Notably, the secondary fraction for OPAHs increased by 10.4 % from 86 % to 96 %, while the secondary fraction for NACs rose by 8.9 % from 90 % before heating to 98 % during heating. Earlier studies have highlighted the presence of significant levels of secondary particle BrC during autumn and winter, particularly during haze periods (Ding et al., 2017; Liu et al., 2023), and the results

Table 2. Correlations between NACs and meteorological parameters, gas pollutants, and aerosol components before ($n = 56$) and during the heating period ($n = 66$).

Before heating period		Levoglucosan	K^+	SO_2	NO_2	O_3	RH	SO_4^{2-}	NO_3^-	NH_4^+
NACs	∑9NACs	0.897**	0.738**	0.210	0.714**	0.692**	0.170	0.359**	0.369**	0.190
	4NP	0.784**	0.699**	0.249	0.715**	0.649**	0.118	0.345**	0.372**	0.207
	3M4NP	0.752**	0.526**	0.290*	0.575**	0.511**	−0.011	0.184	0.191	0.029
	2,4-DNP	0.436**	0.353**	0.310*	0.463**	0.492**	−0.151	0.034	−0.048	−0.166
	4NGA	0.545**	0.361**	0.438**	0.560**	0.524**	−0.137	−0.016	−0.025	−0.131
	5NGA	0.582**	0.355**	0.114	0.343**	0.433**	0.005	0.120	0.139	0.044
	4NC	0.897**	0.748**	0.064	0.641**	0.617**	0.308*	0.448**	0.486**	0.325*
	4M5NC	0.885**	0.668**	0.076	0.579**	0.577**	0.252	0.364**	0.413**	0.261
	3NSA	0.791**	0.678**	0.129	0.553**	0.495**	0.214	0.457**	0.515**	0.331*
	5NSA	0.737**	0.596**	0.219	0.594**	0.553**	0.085	0.279*	0.316*	0.125
During heating period		**Levoglucosan**	**K^+**	**SO_2**	**NO_2**	**O_3**	**RH**	**SO_4^{2-}**	**NO_3^-**	**NH_4^+**
NACs	∑9NACs	0.888**	0.786**	0.275*	0.481**	−0.303*	0.548**	0.373**	0.504**	0.513**
	4NP	0.812**	0.725**	0.262*	0.471**	−0.296*	0.586**	0.390**	0.489**	0.511**
	3M4NP	0.756**	0.655**	0.248	0.374**	−0.225	0.613**	0.318**	0.397**	0.462**
	2,4-DNP	0.537**	0.495**	0.280*	0.417**	−0.304*	0.199	0.136	0.247*	0.136
	4NGA	0.672**	0.406**	0.229	0.274*	−0.206	0.201	−0.047	0.074	0.081
	5NGA	0.275*	0.208	−0.028	0.190	0.026	−0.006	0.114	0.100	0.125
	4NC	0.894**	0.804**	0.248	0.454**	−0.290*	0.520**	0.378**	0.523**	0.530**
	4M5NC	0.882**	0.736**	0.246	0.434**	−0.244	0.430**	0.283*	0.421**	0.422**
	3NSA	0.788**	0.910**	0.348**	0.681**	−0.410**	0.577**	0.707**	0.888**	0.828**
	5NSA	0.820**	0.866**	0.268*	0.629**	−0.377**	0.599**	0.680**	0.846**	0.828**

** Significant correlation at the 0.01 level. * Significant correlation at the 0.05 level.

Table 3. Correlations between OPAHs and meteorological parameters, gas pollutants, and aerosol components before ($n = 56$) and during the heating period ($n = 66$).

Before heating period		∑9NACs	Levoglucosan	K^+	SO_2	NO_2	O_3	RH	SO_4^{2-}	NO_3^-	NH_4^+
OPAHs	∑8OPAHs	0.830**	0.865**	0.605**	0.188	0.563**	0.563**	0.143	0.244	0.283*	0.139
	1-NapA	0.844**	0.870**	0.621**	0.211	0.640**	0.622**	0.174	0.213	0.238	0.096
	9-FO	0.775**	0.785**	0.646**	0.283*	0.558**	0.573**	0.059	0.183	0.235	0.119
	ATQ	0.633**	0.694**	0.497**	0.392**	0.477**	0.483**	−0.018	0.042	0.061	−0.024
	BZA	0.686**	0.759**	0.573**	0.232	0.537**	0.594**	0.110	0.177	0.206	0.117
	7,12-BaAQ	0.821**	0.865**	0.685**	0.189	0.591**	0.622**	0.187	0.325*	0.356**	0.224
	1,4-CQ	0.636**	0.646**	0.406**	0.041	0.303*	0.290*	0.102	0.259	0.309*	0.174
	5,12-NAQ	0.694**	0.752**	0.563**	0.227	0.511**	0.559**	0.091	0.184	0.214	0.110
	BPYRone	0.827**	0.870**	0.662**	0.131	0.590**	0.616**	0.226	0.345**	0.398**	0.255
During heating period		**∑9NACs**	**Levoglucosan**	**K^+**	**SO_2**	**NO_2**	**O_3**	**RH**	**SO_4^{2-}**	**NO_3^-**	**NH_4^+**
OPAHs	∑8OPAHs	0.895**	0.931**	0.877**	0.365**	0.678**	−0.385**	0.578**	0.477**	0.658**	0.658**
	1-NapA	0.752**	0.774**	0.659**	0.248	0.547**	−0.378**	0.332*	0.332**	0.498**	0.446**
	9-FO	0.478**	0.457**	0.342**	0.305*	0.302*	−0.020	0.131	−0.013	0.167	0.250*
	ATQ	0.780**	0.797**	0.815**	0.426**	0.668**	−0.372**	0.656**	0.466**	0.642**	0.684**
	BZA	0.840**	0.881**	0.829**	0.332**	0.570**	−0.273*	0.577**	0.431**	0.568**	0.577**
	7,12-BaAQ	0.801**	0.856**	0.896**	0.391**	0.633**	−0.299*	0.655**	0.531**	0.689**	0.710**
	1,4-CQ	0.703**	0.780**	0.791**	0.244	0.597**	−0.282*	0.624**	0.560**	0.647**	0.675**
	5,12-NAQ	0.777**	0.818**	0.869**	0.365**	0.601**	−0.293*	0.535**	0.444**	0.619**	0.614**
	BPYRone	0.858**	0.857**	0.845**	0.339**	0.588**	−0.320*	0.478**	0.396**	0.612**	0.568**

** Significant correlation at the 0.01 level. * Significant correlation at the 0.05 level.

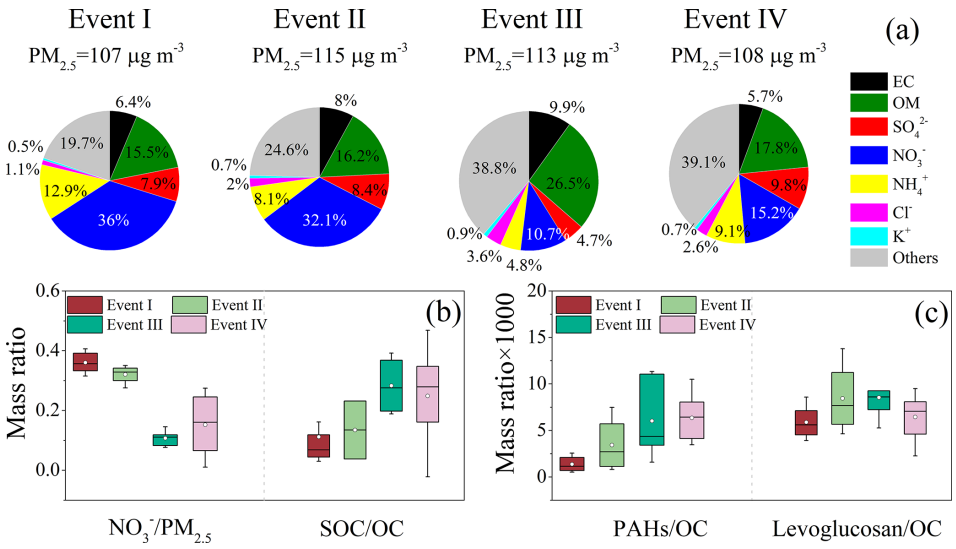

Figure 5. Comparative analysis of the chemical composition of $PM_{2.5}$ during four distinct events of air pollution. **(a)** Relative percentages of major species in $PM_{2.5}$ and **(b, c)** mass ratios of the key species and organic tracers in $PM_{2.5}$. The mean values are represented by the markers, and the 25th and 75th percentiles are represented by whiskers.

of this work corroborate earlier studies well. Moreover, the good correlations between OPAHs and NACs with O_3 before heating and with RH during heating confirm the importance of photochemical and aqueous oxidation in these two different periods.

3.4 Different pollution characteristics in haze events

From Fig. 1, it can be found that $PM_{2.5}$ shows four equivalent maxima lasting for 2 to 5 d. Among the four pollution events, two occurred before heating (24–27 October and 5–6 November), and the other two occurred during heating (18–20 November and 27–31 December). $PM_{2.5}$ was significantly different in terms of its chemical constituents before and during heating, although the mass concentration of $PM_{2.5}$ was rather similar (respectively averaging 107, 115, 113, and 108 $\mu g\,m^{-3}$ for Event I, II, III, and IV) (Fig. 5a). In the two events before heating, OM existed as the second most dominant species in $PM_{2.5}$, with respective relative abundance of 15.5 % and 16.2 % in Events I and II. In contrast, OM surfaced as the most dominant species of $PM_{2.5}$ during heating. The relative abundance of OM (26.5 %) during Event III was higher (17.8 %) than that during Event IV (Fig. 5a). The ratios of NO_3^- / $PM_{2.5}$ were higher in Events I and II as compared to Events III and IV, with the ratios of secondary organic carbon (SOC) / OC showing the opposite trend (Fig. 5b), suggesting a significant increase in the concentration of secondary organic compounds after heating. In the context of fossil fuel combustion, PAHs serve as markers for coal burning, while levoglucosan acts as a significant tracer for biomass smoke. Figure 5c shows that the ratios of PAHs to organic carbon mass in $PM_{2.5}$ (PAHs / OC) were higher during Events III and IV compared to Events I and II. This underscores the heightened emissions from household burning of coal for heating purposes. Levoglucosan / OC, the mass ratio of levoglucosan to OC in $PM_{2.5}$, did not, however, rise considerably over the same period (Fig. 5c), indicating a similar degree of emissions from burning biomass before and during heating. This result was consistent with our earlier research from the 2014 APEC meeting (Wang et al., 2017).

According to the majority of research, Beijing's haze is distinguished by intense secondary formation (Zhang et al., 2018; Xu et al., 2017; Sun et al., 2016; Guo et al., 2014). According to several research studies, organic material (OM) predominates in the autumn and winter, while secondary SIA is the most prevalent species in the summer (Renhe et al., 2014). Additionally, according to a few investigators, SIA has a major role in wintertime pollution episodes (Guo et al., 2014; Wang et al., 2016). Furthermore, a recent investigation identified the species responsible for Beijing haze and listed distinct haze-driving species operative over the year: the haze is primarily OM-driven during winter and late autumn, nitrate-driven in early autumn, and sulfate-driven in summer, whereas it is driven primarily by nitrates during spring (Tan et al., 2018). Table 4 and Fig. 5a depict that $PM_{2.5}$ was enriched with SIA, especially NO_3^-, during Events I and II, but enriched OM with higher levels of SOC was observed during Events III and IV. The findings strongly indicated that haze during autumn and winter in urban Beijing was primarily influenced by nitrate before heating and shifted to being driven by SOC during heating. Table 4 illustrates that T and RH were notably higher during Events I and II compared to Events III and IV. These warmer and moister conditions favored photochemical oxidation, leading to an

Table 4. Meteorological parameters, chemical components ($\mu g\,m^{-3}$) of $PM_{2.5}$, and concentrations of gaseous pollutants (ppb) among four pollution episodes in Beijing.

	Before heating period		During heating period	
	Event I 24–27 October $N = 8$	Event II 5–6 November $N = 4$	Event III 18–20 November $N = 6$	Event IV 27–31 December $N = 10$
$PM_{2.5}$	107 ± 29	115 ± 48	113 ± 37	108 ± 35
Temperature, °C	13 ± 1.6	8.8 ± 4.2	1.8 ± 2.6	1.8 ± 3.8
Relative humidity, %	79 ± 10	55 ± 26	29 ± 10	36 ± 22
SO_2	1.4 ± 0.1	1.9 ± 1.1	5.0 ± 1.0	4.0 ± 1.2
NO	27 ± 19	27 ± 15	51 ± 42	47 ± 31
NO_2	30 ± 6.7	33 ± 14	40 ± 12	37 ± 8.1
SIA[a]	62 ± 20	58 ± 22	23 ± 9.9	39 ± 30
NO_3^-	39 ± 13	38 ± 15	12 ± 5.2	18 ± 14
SOC[b]	1.9 ± 1.3	2.3 ± 1.8	7.0 ± 2.8	3.9 ± 2.5
NACs, $ng\,m^{-3}$	17 ± 8.3	41 ± 36	131 ± 85	55 ± 27
OPAHs, $ng\,m^{-3}$	21 ± 7.6	62 ± 85	127 ± 53	74 ± 23

[a] SIA: secondary inorganic aerosol (the sum of sulfate, nitrate, and ammonium). [b] SOC: secondary organic carbon ($[SOC] = [OC] - [EC] \times ([OC]/[EC])_{pri}$). $([OC]/[EC])_{pri}$ was estimated from the fitting of the minimum [OC] / [EC] ratio, assuming that the primary source dominated the period with minimal secondary formation. In this work, $([OC]/[EC])_{pri}$ was estimated from the fitting of the lowest 15 % [OC] / [EC] ratios during the whole sampling period.

increased abundance of SIA during the same period. Home heating activities, such as burning residential coal, were increased during the heating period. This resulted in massive emissions of SO_2, NO_x, VOCs, and primary particles, all of which were conducive to the generation of SOC. As a result, during Events III and IV, SOC concentrations and relative abundances were higher than during Events I and II. Furthermore, Fig. 6a shows that the NACs / OC and OPAHs / OC ratios were significantly higher in Events III and IV compared to Events I and II. Figure 6b displays a parallel trend in the relative contributions of secondary formation for both events, highlighting a notable increase in the secondary formation of BrC during pollution events, particularly evident during heating periods.

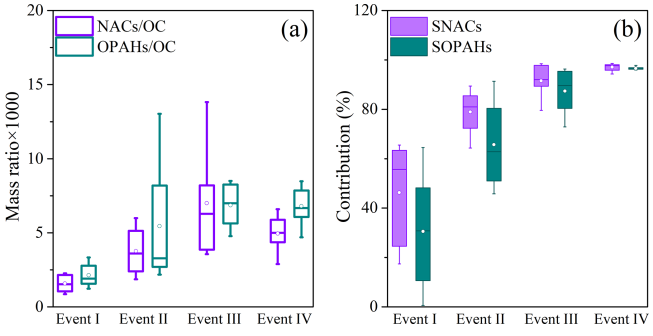

Figure 6. Comparative analysis of the chemical composition of BrC during four distinct air pollution events. **(a)** Mass ratios of NACs and OPAHs to OC in $PM_{2.5}$. **(b)** Relative contributions of secondary formation (SNACs/OPAHs) to the total NACs/OPAHs in the fine particulate matter. The mean values are represented by the markers, and the 25th and 75th percentiles are represented by whiskers.

4 Conclusions

The current study determined the concentrations of nine $PM_{2.5}$-bound NACs and eight $PM_{2.5}$-bound OPAHs in autumn and winter in Beijing urban areas. The OPAH and NAC concentrations were much higher during heating than before heating. These species have a distinct diurnal variation, with higher concentrations at night compared to day. 4-Nitrophenol, 4-nitrocatechol, and 1-naphthaldehyde were the most abundantly existing species in the whole campaign.

The primary sources of NACs and OPAHs were biomass combustion and automobile emissions, with the secondary generation of BrC being the predominant contributor across the entire sampling period. Our results underscore the significant role of secondary generation in producing BrC, particularly its heightened contribution in pollution events during heating. A comparative analysis of the chemical constitution of $PM_{2.5}$ and BrC in four different haze events also revealed that the haze was caused by SOC during heating and by nitrate before heating in autumn and winter. Increased attention should be directed towards reducing the emissions of aromatic hydrocarbons and other anthropogenic volatile organic compounds (VOCs) when heating commences. This focus is crucial for effectively mitigating pollution and ensuring the preservation of human health. There is still only a limited volume of research on the molecular makeup of BrC, and further research is needed to identify more impactful chromophores at a molecular level. Additionally, a comprehen-

sive exploration of the secondary generation pathways and key influencing factors of BrC through field observations and laboratory simulations is essential. This investigation is crucial for accurately assessing the environmental and human health impacts of BrC.

Data availability. The field observational and the lab experimental data used in this study are available from the corresponding author upon request (Hong Li via lihong@craes.org.cn).

Supplement. The supplement related to this article is available online at: https://doi.org/10.5194/acp-24-6525-2024-supplement.

Author contributions. YR, GW, and HL designed the research; YR, YJ, and ZW collected the samples; YR, FB, and HaoZ conducted the experiments; YR and GW analyzed the data; YR wrote the paper; and GW, JL, HaiZ, and HL contributed to the paper with useful scientific discussions and comments.

Competing interests. The contact author has declared that none of the authors has any competing interests.

Disclaimer. Publisher's note: Copernicus Publications remains neutral with regard to jurisdictional claims made in the text, published maps, institutional affiliations, or any other geographical representation in this paper. While Copernicus Publications makes every effort to include appropriate place names, the final responsibility lies with the authors.

Acknowledgements. This work was supported by the Fundamental Research Funds for Central Public Welfare Scientific Research Institutes of China (nos. 2022YSKY-27, 2019YSKY-018, and 2022YSKY-21) and the National Natural Science Foundation of China (nos. 42130704 and 41907197).

Financial support. This research has been supported by the National Key Research and Development Program of China (grant no. 2023YFC3706105), the Fundamental Research Funds for Central Public Welfare Scientific Research Institutes of China (grant nos. 2022YSKY-27, 2019YSKY-018, and 2022YSKY-21), and the National Natural Science Foundation of China (grant nos. 42130704 and 41907197).

Review statement. This paper was edited by Zhibin Wang and reviewed by three anonymous referees.

References

Alves, C., Vicente, A., Custódio, D., Cerqueira, M., Nunes, T., Pio, C., Lucarelli, F., Calzolai, G., Nava, S., and Diapouli, E.: Polycyclic aromatic hydrocarbons and their derivatives (nitro-PAHs, oxygenated PAHs, and azaarenes) in $PM_{2.5}$ from Southern European cities, Sci. Total. Environ., 595, 494–504, https://doi.org/10.1016/j.scitotenv.2017.03.256, 2017.

An, Z., Huang, R. J., Zhang, R., Tie, X., Li, G., Cao, J., Zhou, W., Shi, Z., Han, Y., Gu, Z., and Ji, Y.: Severe haze in northern China: A synergy of anthropogenic emissions and atmospheric processes, P. Natl. Acad. Sci. USA, 116, 8657–8666, https://doi.org/10.1073/pnas.1900125116, 2019.

Bai, X., Wei, J., Ren, Y., Gao, R., Chai, F., Li, H., Xu, F., and Kong, Y.: Pollution characteristics and health risk assessment of Polycyclic aromatic hydrocarbons and Nitrated polycyclic aromatic hydrocarbons during heating season in Beijing, J. Environ. Sci.-China, 123, 169–182, https://doi.org/10.1016/j.jes.2022.02.047, 2023.

Cai, D., Wang, X., George, C., Cheng, T., Herrmann, H., Li, X., and Chen, J.: Formation of Secondary Nitroaromatic Compounds in Polluted Urban Environments, J. Geophys. Res.-Atmos., 127, e2021JD036167, https://doi.org/10.1029/2021JD036167, 2022.

Chen, Y., Zheng, P., Wang, Z., Pu, W., Tan, Y., Yu, C., Xia, M., Wang, W., Guo, J., Huang, D., Yan, C., Nie, W., Ling, Z., Chen, Q., Lee, S., and Wang, T.: Secondary Formation and Impacts of Gaseous Nitro-Phenolic Compounds in the Continental Outflow Observed at a Background Site in South China, Environ. Sci. Technol., 56, 6933–6943, https://doi.org/10.1021/acs.est.1c04596, 2022.

Cheng, X., Chen, Q., Li, Y., Huang, G., Liu, Y., Lu, S., Zheng, Y., Qiu, W., Lu, K., Qiu, X., Bianchi, F., Yan, C., Yuan, B., Shao, M., Wang, Z., Canagaratna, M., Zhu, T., Wu, Y., and Zeng, L.: Secondary Production of Gaseous Nitrated Phenols in Polluted Urban Environments, Environ. Sci. Technol., 55, 4410–4419, https://doi.org/10.1021/acs.est.0c07988, 2021.

Chow, K. S., Huang, X. H. H., and Yu, J. Z.: Quantification of nitroaromatic compounds in atmospheric fine particulate matter in Hong Kong over 3 years: field measurement evidence for secondary formation derived from biomass burning emissions, Environ. Chem., 13, 665–673, https://doi.org/10.1071/EN15174, 2016.

Claeys, M., Vermeylen, R., Yasmeen, F., Gómez-González, Y., Chi, X., Maenhaut, W., Mészáros, T., and Salma, I.: Chemical characterisation of humic-like substances from urban, rural and tropical biomass burning environments using liquid chromatography with UV/vis photodiode array detection and electrospray ionisation mass spectrometry, Environ. Chem., 9, 273–284, 2012.

Ding, X., Zhang, Y. Q., He, Q., Yu, Q. Q., Wang, J. Q., Shen, R. Q., Song, W., Wang, Y., and Wang, X.: Significant increase of aromatics-derived secondary organic aerosol during fall to winter in China, Environ. Sci. Technol., 13, 7432–7441, https://doi.org/10.1021/acs.est.6b06408, 2017.

Du, Z., He, K., Cheng, Y., Duan, F., Ma, Y., Liu, J., Zhang, X., Zheng, M., and Weber, R.: A yearlong study of water-soluble organic carbon in Beijing II: Light absorption properties, Atmos. Environ., 89, 235–241, https://doi.org/10.1016/j.atmosenv.2014.02.022, 2014.

Fan, X., Peng, P., and Song, J.: Temporal variations of the abundance and optical properties of water soluble Humic-Like Substances (HULIS) in $PM_{2.5}$ at Guangzhou, China, Atmos. Res., 172–173, 8–15, https://doi.org/10.1016/j.atmosres.2015.12.024, 2016.

Finewax, Z., Gouw, J., and Ziemann, P.: Identification and Quantification of 4-Nitrocatechol Formed from OH and NO_3 Radical-Initiated Reactions of Catechol in Air in the Presence of NO_x: Implications for Secondary Organic Aerosol Formation from Biomass Burning, Environ. Sci. Technol., 52, 1981–1989, https://doi.org/10.1021/acs.est.7b05864, 2018.

Guo, S., Hu, M., Zamora, M. L., Peng, J., Shang, D., Zheng, J., Du, Z., Wu, Z., Shao, M., and Zeng, L.: Elucidating severe urban haze formation in China, P. Natl. Acad. Sci. USA., 111, 17373–17378, https://doi.org/10.1073/pnas.1419604111, 2014.

Huang, R. J., Yang, L., Cao, J., Chen, Y., Chen, Q., Li, Y., Duan, J., Zhu, C., Dai, W., Wang, K., Lin, C., Ni, H., Corbin, J. C., Wu, Y., Zhang, R., Tie, X., Hoffmann, T., O'Dowd, C., and Dusek, U.: Brown Carbon Aerosol in Urban Xi'an, Northwest China: The Composition and Light Absorption Properties, Environ. Sci. Technol., 52, 6825–6833, https://doi.org/10.1021/acs.est.8b02386, 2018.

Iinuma, Y., Boge, O., Graefe, R., and Herrmann, H.: Methyl-Nitrocatechols: Atmospheric Tracer Compounds for Biomass Burning Secondary Organic Aerosols, Environ. Sci. Technol., 44, 8453, https://doi.org/10.1021/es102938a, 2010.

Ji, Y., Zhao, J., Terazono, H., Misawa, K., and Zhang, R.: Reassessing the atmospheric oxidation mechanism of toluene, P. Natl. Acad. Sci. USA, 114, 8169–8174, https://doi.org/10.1073/pnas.1705463114, 2017.

Jiang, H., Cai, J., Feng, X., Chen, Y., Wang, L., Li, J., Tang, J., Mo, Y., Zhang, X., Zhang, G., Mu, Y., and Chen, J.: Aqueous-Phase Secondary Processes and Meteorological Change Promote the Brown Carbon Formation and Transformation During Haze Events, J. Geophys. Res.-Atmos., 128, e2023JD038735, https://doi.org/10.1029/2023JD038735, 2023.

Kahnt, A., Behrouzi, S., Vermeylen, R., Shalamzari, M. S., Vercauteren, J., Roekens, E., Claeys, M., and Maenhaut, W.: One-year study of nitro-organic compounds and their relation to wood burning in PM_{10} aerosol from a rural site in Belgium, Atmos. Environ., 81, 561–568, https://doi.org/10.1016/j.atmosenv.2013.09.041, 2013.

Kitanovski, Z., Shahpoury, P., Samara, C., Voliotis, A., and Lammel, G.: Composition and mass size distribution of nitrated and oxygenated aromatic compounds in ambient particulate matter from southern and central Europe – implications for the origin, Atmos. Chem. Phys., 20, 2471–2487, https://doi.org/10.5194/acp-20-2471-2020, 2020.

Lammel, G., Kitanovski, Z., Kukucka, P., Novák, J., and Wietzoreck, M.: Oxygenated and nitrated polycyclic aromatic hydrocarbons (OPAHs, NPAHs) in ambient air – levels, phase partitioning, mass size distributions and inhalation bioaccessibility, Environ. Sci. Technol., 54, 2615–2625, https://doi.org/10.1021/acs.est.9b06820, 2020.

Laskin, A., Laskin, J., and Nizkorodov, S. A.: Chemistry of atmospheric brown carbon, Chem. Rev., 115, 4335–4382, https://doi.org/10.1021/cr5006167, 2015.

Li, J., Wang, G., Ren, Y., Wang, J., Wu, C., Han, Y., Zhang, L., Cheng, C., and Meng, J.: Identification of chemical compositions and sources of atmospheric aerosols in Xi'an, inland China during two types of haze events, Sci. Total. Environ., 566, 230–237, https://doi.org/10.1016/j.scitotenv.2016.05.057, 2016.

Li, J., Zhang, Q., Wang, G., Li, J., Wu, C., Liu, L., Wang, J., Jiang, W., Li, L., Ho, K. F., and Cao, J.: Optical properties and molecular compositions of water-soluble and water-insoluble brown carbon (BrC) aerosols in northwest China, Atmos. Chem. Phys., 20, 4889–4904, https://doi.org/10.5194/acp-20-4889-2020, 2020.

Li, X., Han, J., Hopke, P. K., Hu, J., Shu, Q., Chang, Q., and Ying, Q.: Quantifying primary and secondary humic-like substances in urban aerosol based on emission source characterization and a source-oriented air quality model, Atmos. Chem. Phys., 19, 2327–2341, https://doi.org/10.5194/acp-19-2327-2019, 2019.

Li, X., Yang, Y., Liu, S., Zhao, Q., Wang, G., and Wang, Y.: Light absorption properties of brown carbon (BrC) in autumn and winter in Beijing: Composition, formation and contribution of nitrated aromatic compounds, Atmos. Environ., 223, 117289, https://doi.org/10.1016/j.atmosenv.2020.117289, 2020.

Li, Y., Bai, X., Ren, Y., Gao, R., Ji, Y., Wang, Y., and Li, H.: PAHs and nitro-PAHs in urban Beijing from 2017 to 2018: Characteristics, sources, transformation mechanism and risk assessment, J. Hazard. Mater., 436, 1–11, https://doi.org/10.1016/j.jhazmat.2022.129143, 2022.

Liu, J., Mo, Y., Ding, P., Li, J., Shen, C., and Zhang, G.: Dual carbon isotopes (14C and 13C) and optical properties of WSOC and HULIS-C during winter in Guangzhou, China, Sci. Total. Environ., 633, 1571–1578, https://doi.org/10.1016/j.scitotenv.2018.03.293, 2018.

Liu, X., Wang, H., Wang, F., Lv, S., Wu, C., Zhao, Y., Zhang, S., Liu, S., Xu, X., Lei, Y., and Wang, G.: Secondary Formation of Atmospheric Brown Carbon in China Haze: Implication for an Enhancing Role of Ammonia, Environ. Sci. Technol., 57, 11163–11172, https://doi.org/10.1021/acs.est.3c03948, 2023.

Lu, C., Wang, X., Dong, S., Zhang, J., and Wang, W.: Emissions of fine particulate nitrated phenols from various on-road vehicles in China, Environ. Res., 179, 108709, https://doi.org/10.1016/j.envres.2019.108709, 2019a.

Lu, C., Wang, X., Li, R., Gu, R., Zhang, Y., Li, W., Gao, R., Chen, B., Xue, L., and Wang, W.: Emissions of fine particulate nitrated phenols from residential coal combustion in China, Atmos. Environ., 203, 10–17, https://doi.org/10.1016/j.atmosenv.2019.01.047, 2019b.

Ma, Y., Cheng, Y., Qiu, X., Cao, G., Fang, Y., Wang, J., Zhu, T., Yu, J., and Hu, D.: Sources and oxidative potential of water-soluble humic-like substances ($HULIS_{WS}$) in fine particulate matter ($PM_{2.5}$) in Beijing, Atmos. Chem. Phys., 18, 5607–5617, https://doi.org/10.5194/acp-18-5607-2018, 2018.

Mohr, C., Lopez-Hilfiker, F. D., Zotter, P., Prévôt, A. S. H., Xu, L., Ng, N. L., Herndon, S. C., Williams, L. R., Franklin, J. P., Zahniser, M. S., Worsnop, D. R., Knighton, W. B., Aiken, A. C., Gorkowski, K. J., Dubey, M. K., Allan, J. D., and Thornton, J. A.: Contribution of Nitrated Phenols to Wood Burning Brown Carbon Light Absorption in Detling, United Kingdom during Winter Time, Environ. Sci. Technol., 47, 6316–6324, https://doi.org/10.1021/es400683v, 2013.

Ni, H., Huang, R. J., Pieber, S. M., Corbin, J. C., and Dusek, U.: Brown Carbon in Primary and Aged Coal Combustion Emission, Environ. Sci. Technol., 55, 5701–5710, https://doi.org/10.1021/acs.est.0c08084, 2021.

Olariu, R. I., Klotz, B. R., Barnes, I., Becker, K. H., and Mocanu, R.: FT-IR study of the ring-retaining products from the reaction of OH radicals with phenol, o-, m-, and p-cresol, Atmos. Environ., 36, 3685–3697, https://doi.org/10.1016/S1352-2310(02)00202-9, 2002.

Ren, Y., Zhou, B., Tao, J., Cao, J., Zhang, Z., Wu, C., Wang, J., Li, J., Zhang, L., Han, Y., Liu, L., Cao, C., and Wang, G.: Composition and size distribution of airborne particulate PAHs and oxygenated PAHs in two Chinese megacities, Atmos. Res., 183, 322–330, https://doi.org/10.1016/j.atmosres.2020.105412, 2017.

Ren, Y., Wei, J., Wu, Z., Ji, Y., Bi, F., Gao, R., Wang, X., Wang, G., and Li, H.: Chemical components and source identification of $PM_{2.5}$ in non-heating season in Beijing: The influences of biomass burning and dust, Atmos. Res., 251, 105412, https://doi.org/10.1016/j.atmosres.2020.105412, 2021.

Ren, Y., Wei, J., Wang, G., Wu, Z., Ji, Y., and Li, H.: Evolution of aerosol chemistry in Beijing under strong influence of anthropogenic pollutants: Composition, sources, and secondary formation of fine particulate nitrated aromatic compounds, Environ. Res., 204, 111982, https://doi.org/10.1016/j.envres.2021.111982, 2022.

Ren, Y., Wang, G., Wei, J., Tao, J., Zhang, Z., and Li, H.: Contributions of primary emissions and secondary formation to nitrated aromatic compounds in themountain background region of Southeast China, Atmos. Chem. Phys., 23, 6835–6848, https://doi.org/10.5194/acp-23-6835-2023, 2023.

Renhe, Z., Qiang, L. I., and Ruonan, Z.: Meteorological conditions for the persistent severe fog and haze event over eastern China in January 2013, Sci. China Earth Sci., 57, 26–35, https://doi.org/10.1007/s11430-013-4774-3, 2014.

Sato, K., Hatakeyama, S., and Imamura, T.: Secondary Organic Aerosol Formation during the Photooxidation of Toluene: NO_x Dependence of Chemical Composition, J. Phys. Chem. A, 111, 9796–9808, https://doi.org/10.1021/jp071419f, 2007.

Song, J., Zhu, M., Wei, S., Peng, P. A., and Ren, M.: Abundance and 14C-based source assessment of carbonaceous materials in $PM_{2.5}$ aerosols in Guangzhou, South China, Atmos. Pollut. Res., 10, 313–320, https://doi.org/10.1016/j.apr.2018.09.003, 2018.

Song, J., Li, M., and Zou, C.: Molecular characterization of nitrogen-containing compounds in humic-like substances emitted from biomass burning and coal combustion, Environ. Sci. Technol., 56, 119–130, https://doi.org/10.1021/acs.est.1c04451, 2022.

Sun, Y., Du, W., Fu, P., Wang, Q., Li, J., Ge, X., Zhang, Q., Zhu, C., Ren, L., Xu, W., Zhao, J., Han, T., Worsnop, D. R., and Wang, Z.: Primary and secondary aerosols in Beijing in winter: sources, variations and processes, Atmos. Chem. Phys., 16, 8309–8329, https://doi.org/10.5194/acp-16-8309-2016, 2016.

Sun, Y. L., Wang, Z. F., Fu, P. Q., Yang, T., Jiang, Q., Dong, H. B., Li, J., and Jia, J. J.: Aerosol composition, sources and processes during wintertime in Beijing, China, Atmos. Chem. Phys., 13, 4577–4592, https://doi.org/10.5194/acp-13-4577-2013, 2013.

Tan, J., Xiang, P., Zhou, X., Duan, J., Ma, Y., He, K., Cheng, Y., Yu, J., and Querol, X.: Chemical characterization of humic-like substances (HULIS) in $PM_{2.5}$ in Lanzhou, China, Sci. Total. Environ., 573, 1481–1490, https://doi.org/10.1016/j.scitotenv.2016.08.025, 2016.

Tan, T., Hu, M., Li, M., Guo, Q., Wu, Y., Fang, X., Gu, F., Wang, Y., and Wu, Z.: New insight into $PM_{2.5}$ pollution patterns in Beijing based on one-year measurement of chemical compositions, Sci. Total. Environ., 621, 734–743, https://doi.org/10.1016/j.scitotenv.2017.11.208, 2018.

Teich, M., Pinxteren, D. V., Kecorius, S., Wang, Z., and Herrmann, H.: First Quantification of Imidazoles in Ambient Aerosol Particles: Potential Photosensitizers, Brown Carbon Constituents, and Hazardous Components, Environ. Sci. Technol., 50, 1166–1173, https://doi.org/10.1021/acs.est.5b05474 2016.

Teich, M., van Pinxteren, D., Wang, M., Kecorius, S., Wang, Z., Müller, T., Močnik, G., and Herrmann, H.: Contributions of nitrated aromatic compounds to the light absorption of water-soluble and particulate brown carbon in different atmospheric environments in Germany and China, Atmos. Chem. Phys., 17, 1653–1672, https://doi.org/10.5194/acp-17-1653-2017, 2017.

Wang, G., Kawamura, K., Xie, M., Hu, S., Gao, S., Cao, J., An, Z., and Wang, Z.: Size-distributions of n-alkanes, PAHs and hopanes and their sources in the urban, mountain and marine atmospheres over East Asia, Atmos. Chem. Phys., 9, 8869–8882, https://doi.org/10.5194/acp-9-8869-2009, 2009.

Wang, G., Zhang, R., Gomez, M. E., Yang, L., Levy, Z. M., Hu, M., Lin, Y., Peng, J., Guo, S., and Meng, J.: Persistent sulfate formation from London Fog to Chinese haze, P. Natl. Acad. Sci. USA, 113, 13630–13635, https://doi.org/10.1073/pnas.1616540113, 2016.

Wang, H., Gao, Y., Wang, S., Wu, X., Liu, Y., Li, X., Dandan, Huang, Lou, S., Wu, Z., Guo, S., Jing, S., Li, Y., Huang, C., Tyndall, G. S., Orlando, J. J., and Zhang, X.: Atmospheric Processing of Nitrophenols and Nitrocresols From Biomass Burning Emissions, J. Geophys. Res.-Atmos., 125, e2020JD033401, https://doi.org/10.1029/2020JD033401, 2020.

Wang, J., Wang, G., Gao, J., Wang, H., Ren, Y., Li, J., Zhou, B., Wu, C., Zhang, L., Wang, S., and Chai, F.: Concentrations and stable carbon isotope compositions of oxalic acid and related SOA in Beijing before, during, and after the 2014 APEC, Atmos. Chem. Phys., 17, 981–992, https://doi.org/10.5194/acp-17-981-2017, 2017.

Wang, L., Wang, X., Gu, R., Wang, H., Yao, L., Wen, L., Zhu, F., Wang, W., Xue, L., Yang, L., Lu, K., Chen, J., Wang, T., Zhang, Y., and Wang, W.: Observations of fine particulate nitrated phenols in four sites in northern China: concentrations, source apportionment, and secondary formation, Atmos. Chem. Phys., 18, 4349–4359, https://doi.org/10.5194/acp-18-4349-2018, 2018.

Wang, Y., Hu, M., Wang, Y., Zheng, J., Shang, D., Yang, Y., Liu, Y., Li, X., Tang, R., Zhu, W., Du, Z., Wu, Y., Guo, S., Wu, Z., Lou, S., Hallquist, M., and Yu, J. Z.: The formation of nitro-aromatic compounds under high NO_x and anthropogenic VOC conditions in urban Beijing, China, Atmos. Chem. Phys., 19, 7649–7665, https://doi.org/10.5194/acp-19-7649-2019, 2019.

Wang, Y., Hu, M., Li, X., and Xu, N.: Chemical Composition, Sources and Formation Mechanisms of Particulate Brown Carbon in the Atmosphere (in Chinese), Prog. Chem., 32, 627–645, https://doi.org/10.7536/PC190917, 2020a.

Wang, Y., Mehra, A., Krechmer, J. E., Yang, G., and Wang, L.: Oxygenated products formed from OH-initiated reactions of trimethylbenzene: Autoxidation and accretion, Atmos. Chem. Phys., 20, 9563-9579, https://doi.org/10.5194/acp-20-9563-2020, 2020b.

Wu, C., Wang, G., Li, J., Li, J., Cao, C., Ge, S., Xie, Y., Chen, J., Li, X., Xue, G., Wang, X., Zhao, Z., and Cao, F.: The characteristics

of atmospheric brown carbon in Xi'an, inland China: sources, size distributions and optical properties, Atmos. Chem. Phys., 20, 2017–2030, https://doi.org/10.5194/acp-20-2017-2020, 2020.

Xie, M., Chen, X., Hays, M., Lewandowski, M., Offenberg, J. H., Kleindienst, T. E., and Holder, A. L.: Light Absorption of Secondary Organic Aerosol: Composition and Contribution of Nitroaromatic Compounds, Environ. Sci. Technol., 51, 11607–11616, https://doi.org/10.1021/acs.est.7b03263, 2017.

Xu, L., Duan, F., He, K., Ma, Y., Zhu, L., Zheng, Y., Huang, T., Kimoto, T., Ma, T., and Li, H.: Characteristics of the secondary water-soluble ions in a typical autumn haze in Beijing, Environ. Pollut., 227, 296–305, https://doi.org/10.1016/j.envpol.2017.04.076, 2017.

Yan, J., Wang, X., Gong, P., Wang, C., and Cong, Z.: Review of brown carbon aerosols: Recent progress and perspectives, Sci. Total. Environ., 634, 1475–1485, https://doi.org/10.1016/j.scitotenv.2018.04.083, 2018.

Yuan, B., Liggio, J., Wentzell, J., Li, S.-M., Stark, H., Roberts, J. M., Gilman, J., Lerner, B., Warneke, C., Li, R., Leithead, A., Osthoff, H. D., Wild, R., Brown, S. S., and de Gouw, J. A.: Secondary formation of nitrated phenols: insights from observations during the Uintah Basin Winter Ozone Study (UBWOS) 2014, Atmos. Chem. Phys., 16, 2139–2153, https://doi.org/10.5194/acp-16-2139-2016, 2016.

Zhang, J., Yuan, Q., Liu, L., Wang, Y., Zhang, Y., Xu, L., Pang, Y., Zhu, Y., Niu, H., Shao, L., Yang, S., Liu, H., Pan, X., Shi, Z., Hu, M., Fu, P., and Li, W.: Trans-Regional Transport of Haze Particles From the North China Plain to Yangtze River Delta During Winter, J. Geophys. Res.-Atmos., 126, e2020JD033778, https://doi.org/10.1029/2020jd033778, 2021.

Zhang, J., Li, W., Wang, Y., Teng, X., Zhang, Y., Xu, L., Yuan, Q., Wu, G., Niu, H., and Shao, L.: Structural Collapse and Coating Composition Changes of Soot Particles During Long-Range Transport, J. Geophys. Res.-Atmos., 128, e2023JD038871, https://doi.org/10.1029/2023jd038871, 2023.

Zhang, Q., Shen, Z., Zhang, L., Zeng, Y., and Cao, J. J.: Investigation of Primary and Secondary Particulate Brown Carbon in Two Chinese Cities of Xi'an and Hong Kong in Wintertime, Environ. Sci. Technol., 54, 3803–3813, https://doi.org/10.1021/acs.est.9b05332, 2020.

Zhang, R., Wang, G., Guo, S., Zamora, M. L., Ying, Q., Lin, Y., Wang, W., Hu, M., and Wang, Y.: Formation of Urban Fine Particulate Matter, Chem. Rev., 115, 3803–3855, 2015.

Zhang, R., Sun, X., Huang, Y., Shi, A., Yan, J., Nie, T., Yan, X., and Li, X.: Secondary inorganic aerosols formation during haze episodes at an urban site in Beijing, China, Atmos. Environ., 177, 275–282, https://doi.org/10.1016/j.atmosenv.2017.12.031, 2018.

Zhang, W., Wang, W., Li, J., Ma, S., and Ge, M.: Light absorption properties and potential sources of brown carbon in Fenwei Plain during winter 2018–2019, J. Environ. Sci.-China, 102, 53–63, https://doi.org/10.1016/j.jes.2020.09.007, 2021.

Zhao, M., Qiao, T., Li, Y., Tang, X., Xiu, G., and Yu, J.: Temporal variations and source apportionment of Hulis-C in $PM_{2.5}$ in urban Shanghai, Sci. Total. Environ., 571, 18–26, https://doi.org/10.1016/j.scitotenv.2016.07.127, 2016.

Zhu, C. S., Qu, Y., Zhou, Y., Huang, H., and Cao, J. J.: High light absorption and radiative forcing contributions of primary brown carbon and black carbon to urban aerosol, Gondwana Res., 90, 159–164, https://doi.org/10.1016/j.gr.2020.10.016, 2021.